Supporting Information

Carbon dots@metal–organic frameworks as dual-functional fluorescent sensors for Fe^{3+} ions and nitro explosives

Yufang Tao,[a,b]+ Yansong Jiang,[a]+ Yating Huang,[a] Junning Liu,[c] Ping Zhang,[a] Xiaodong Chen,[a] Yong Fan,[a] Li Wang*[a] and Jianing Xu*[a]

a *College of Chemistry, Jilin University, Changchun 130012, P. R. China*

b *Shanghai New Epoch High School, Ruian 325206, P. R. China*

c *State Key Laboratory of Supramolecular Structure and Materials, College of Chemistry, Jilin University, Changchun 130012, P. R. China*

+ These authors contributed equally to this work.

Email: lwang99@jlu.edu.cn; xujn@jlu.edu.cn

Table of Contents

Fig. S1 (a) The coordination environment of Cd^{2+} ion center in **1**. (b) The coordination mode of HL^{2-} ligand. S5

Fig. S2 (a) The coordination environment of $Cd1^{2+}$ ion and $Cd2^{2+}$ ion in **2**. (b) The coordination mode of L^{3-} ligand. S6

Fig. S3 TEM image (a), PXRD pattern (b), FT-IR spectrum (c) and UV-vis spectrum (d) of CDs. S7

Fig. S4 Powder X-ray diffraction patterns of compounds. S8

Fig. S5 Powder X-ray diffraction patterns of compounds. S9

Fig. S6 TGA curve of **1** and **2** measured in air atmosphere. S10

Fig. S7 SEM images of **1** (a) and **2** (b). TEM images of Eu^{3+}/CDs@**1** (c) and Eu^{3+}/CDs+**2** (d). S11

Fig. S8 The XPS spectra of CDs, **1**, CDs@**1**, Eu^{3+}/CDs@**1** (a) and CDs, **2**, CDs@**2**, Eu^{3+}/CDs+**2** (b). S12

Fig. S9 FT-IR spectra of compounds. S13

Fig. S10 Representative EDS plot of **1A**. S14

Fig. S11 EDS mapping images of **1A**. S15

Fig. S12 Representative EDS plot of **2A**. S16

Fig. S13 EDS mapping images of **2A**. S17

Fig. S14 Solid-state UV-vis absorption spectra of CDs (a), **1** (b), **2** (c), CDs@**1** (d), CDs+**2** (e), **1A** (f) and **2A** (g) at room temperature. S18

Fig. S15 Solid-state excitation and emission spectra of H_3L (a), CDs (b), **1** (c), **2** (d), CDs@**1** (e), CDs+**2** (f), **1A** (g) and **2A** (h) at room temperature. S19

Fig. S16 Fluorescence decay profiles of CDs (a), **1** (b), **2** (c), CDs@**1** (d), CDs+**2** (e), **1A** (f) and **2A** (g) recorded at room temperature. S20

Fig. S17 Powder X-ray diffraction patterns of **1A** and **2A** after the treatment in different pH conditions. S21

Fig. S18 (a) and (b) The fluorescence intensities of **1A** and **2A** at 612 nm at the addition of various metal ions followed by Fe^{3+} ions. S22

Fig. S19 (a) Relation of fluorescence intensity against Fe^{3+} added into **1A** suspension and their linear fitting curve for the estimation of LOD. S23

Fig. S20 Cyclic response of **1A** and **2A** for sensing Fe^{3+} (fluorescence intensity at 612 nm. S24

Fig. S21 PXRD patterns of **1A** and **2A** after cyclic sensing Fe^{3+} ions and nitro explosives. S25

Fig. S22 Variation of fluorescence intensity of **1A** and **2A** with immersion time in analyte solution of Fe^{3+} (1×10^{-2} M^{-1}). S26

Fig. S23 Effect of pH on the emission intensity of **1A** and **2A** in the presence of Fe^{3+} ions. S27

Fig. S24 (a) and (b)The fluorescence intensities of **8A** and **9A** at 612 nm at the addition of various nitro explosives followed by *p*-NT and 2,4-DNP, respectively. S28

Fig. S25 (a) Relation of fluorescence intensity against *p*-NT added into **8A** suspension and their linear fitting curve for the estimation of LOD. S29

Fig. S26 Cyclic response of **1A** and **2A** for sensing *p*-NT and 2,4-DNP, respectively. (fluorescence intensity at 612 nm). S30

Fig. S27 (a) and (b) The absorption spectra of different cations and the excitation spectrum of **1A** and **2A**. S31

Fig. S28 Fluorescence decay profiles of Fe^{3+}@**1A** (a) and Fe^{3+}@**2A** (b) recorded at room temperature. S32

Fig. S29 Sensitivity of (a) **1A** and CDs@**1**, (b) **2A** and CDs+**2**. S33

Fig. S30 (a) and (b) The absorption spectra of different nitro explosives and the excitation spectrum of **1A** and **2A**. S34

Fig. S31 The UV–vis absorption spectra of **1A** and *p*-NT@**1A** (a), **2A** and 2,4-DNP@**2A** (b). S35

Table S1 Crystal data and structure refinement for **1** and **2**. S36

Table S2 Selected bond lengths [Å] and angles [°] for **1** and **2**. S37

Table S3 Fluorescence lifetimes of CDs, **1**, **2**, CDs@**1**, CDs+**2**, **1A**, **2A**, S39

Fe^{3+}@**1A** and Fe^{3+}@**2A**.

Table S4 The comparison of K_{SV} and detection limit between **1A** and **2A** and other reported fluorescent chemosensors for detecting of Fe^{3+} ions. S40

Table S5 The comparison of K_{SV} and detection limit between **1A** and other reported fluorescent chemosensors for detecting of *p*-NT. S41

Table S6 The comparison of K_{SV} and detection limit between **2A** and other reported fluorescent chemosensors for the detecting of 2,4-DNP. S42

References S43

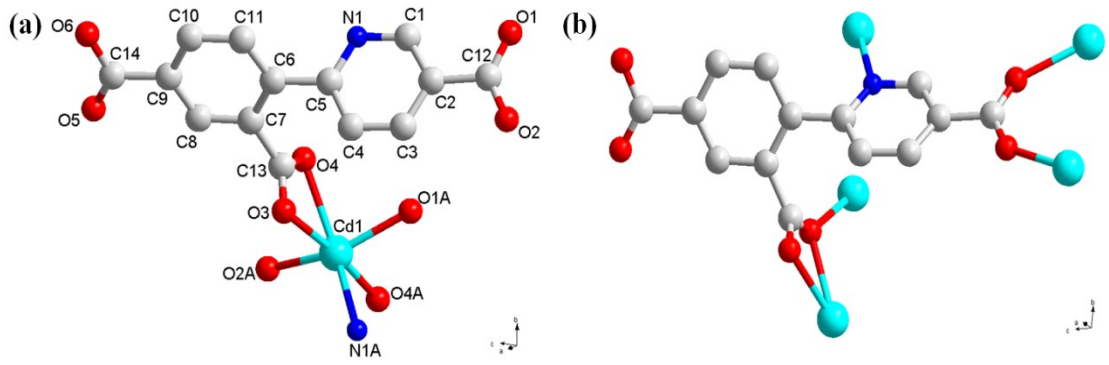

Fig. S1 (a) The coordination environment of Cd^{2+} ion center in **1**. (b) The coordination mode of HL^{2-} ligand.

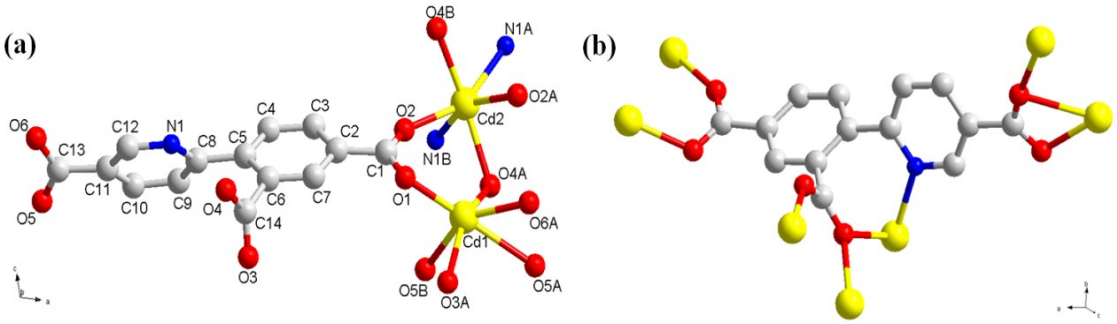

Fig. S2 (a) The coordination environment of $Cd1^{2+}$ ion and $Cd2^{2+}$ ion in **2**. (b) The coordination mode of L^{3-} ligand.

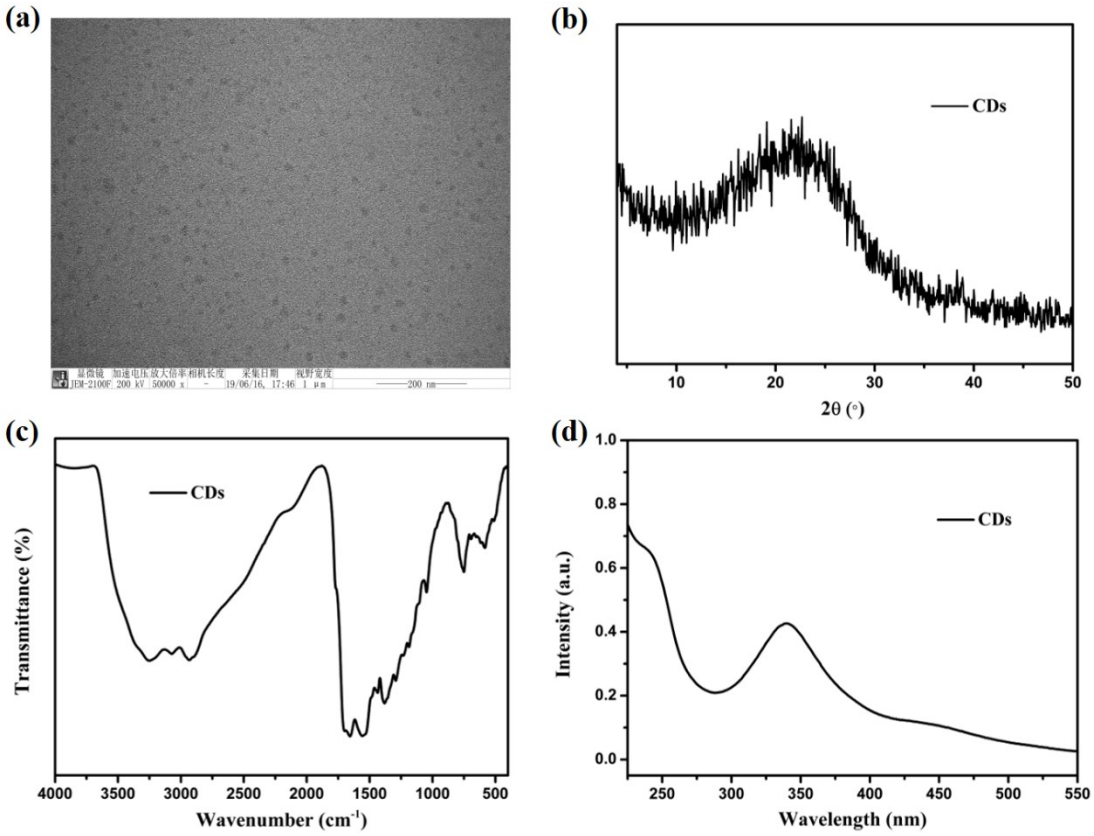

Fig. S3 TEM image (a), PXRD pattern (b), FT-IR spectrum (c) and UV-vis spectrum (d) of CDs.

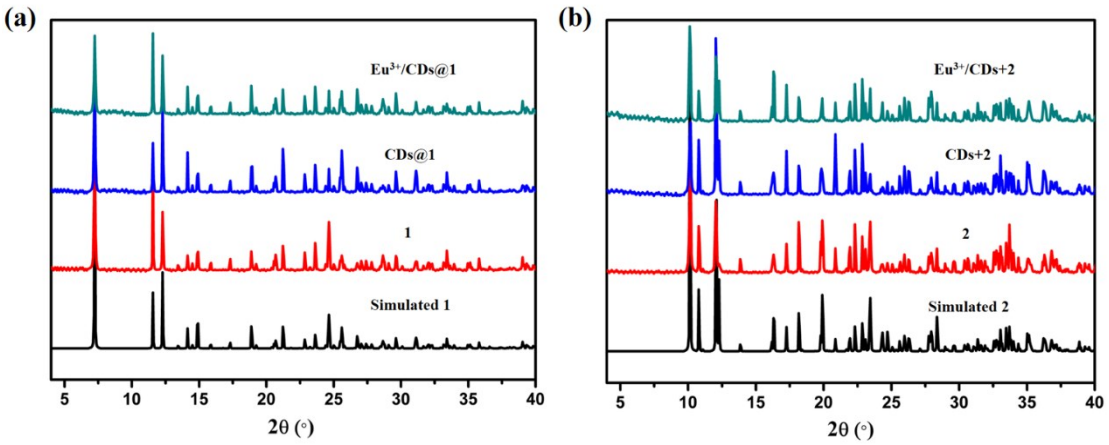

Fig. S4 Powder X-ray diffraction patterns of compounds.

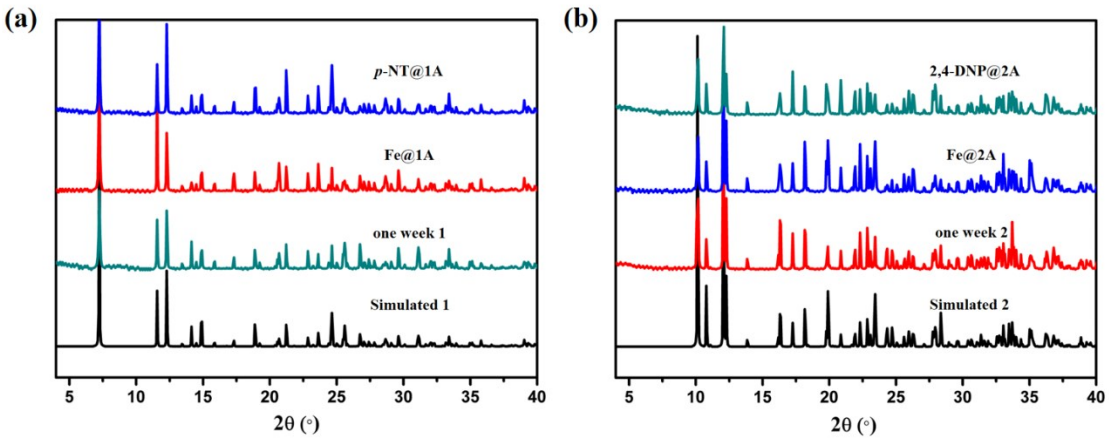

Fig. S5 Powder X-ray diffraction patterns of compounds.

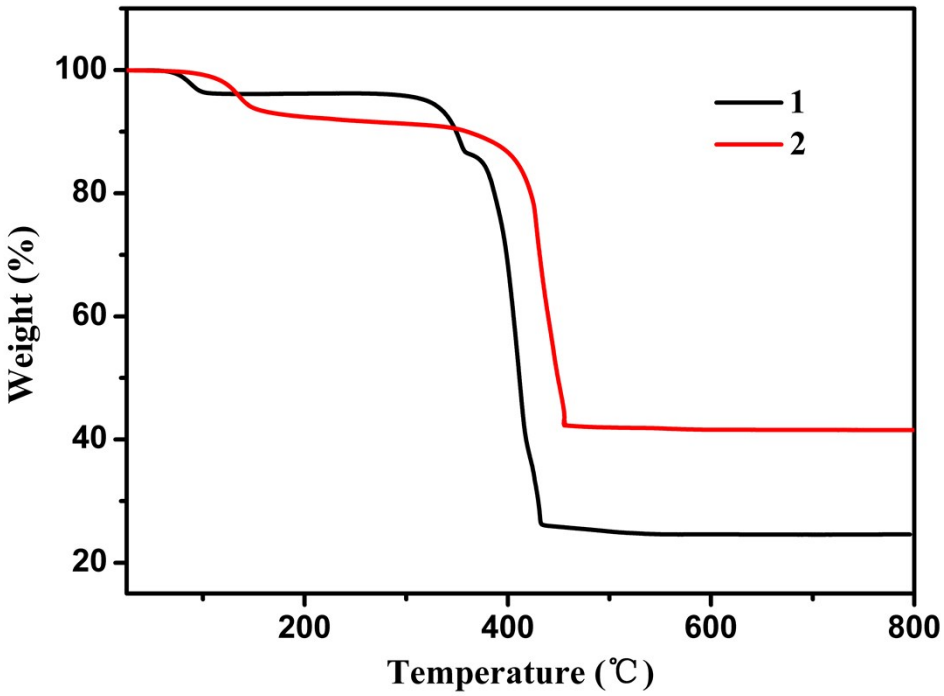

Fig. S6 TGA curve of **1** and **2** measured in air atmosphere.

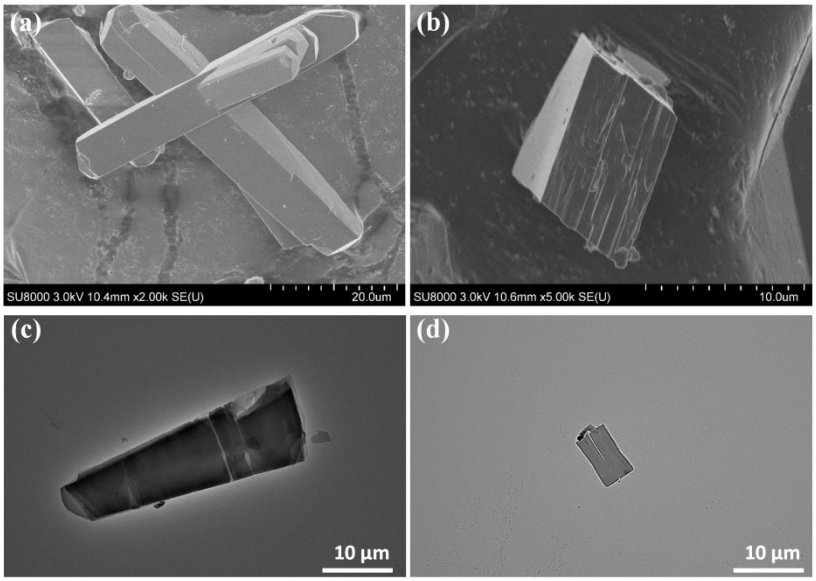

Fig. S7 SEM images of **1** (a) and **2** (b). TEM images of Eu^{3+}/CDs@**1** (c) and Eu^{3+}/CDs+**2** (d).

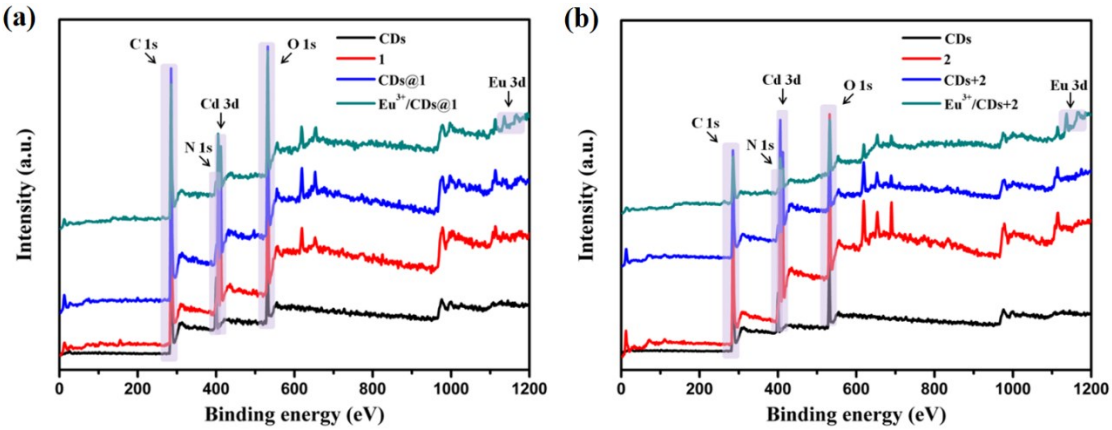

Fig. S8 The XPS spectra of CDs, **1**, CDs**@1**, Eu^{3+}/CDs**@1** (a) and CDs, **2**, CDs**@2**, Eu^{3+}/CDs+**2** (b).

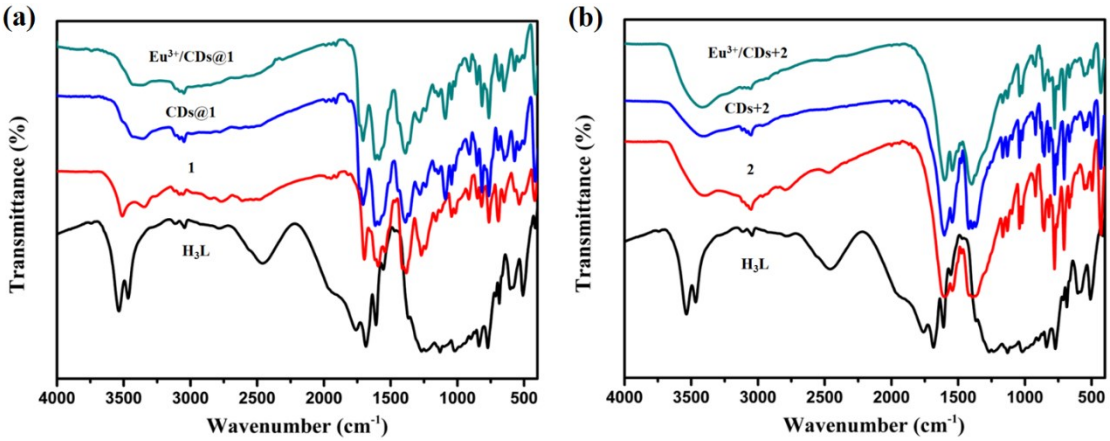

Fig. S9 FT-IR spectra of compounds.

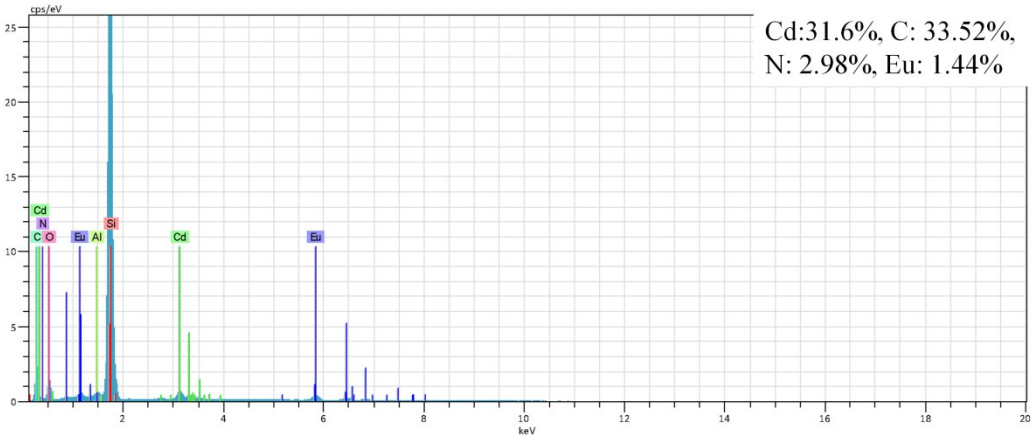

Fig. S10 Representative EDS plot of **1A**.

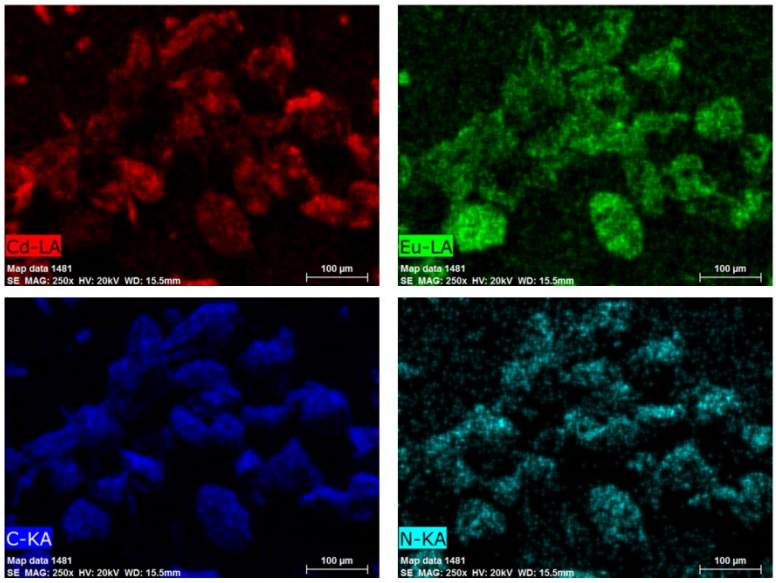

Fig. S11 EDS mapping images of **1A**.

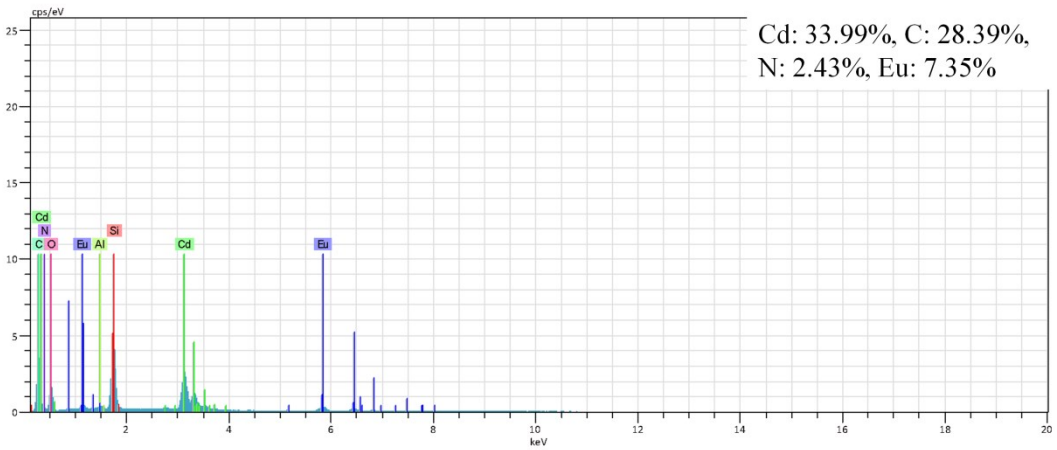

Fig. S12 Representative EDS plot of **2A**.

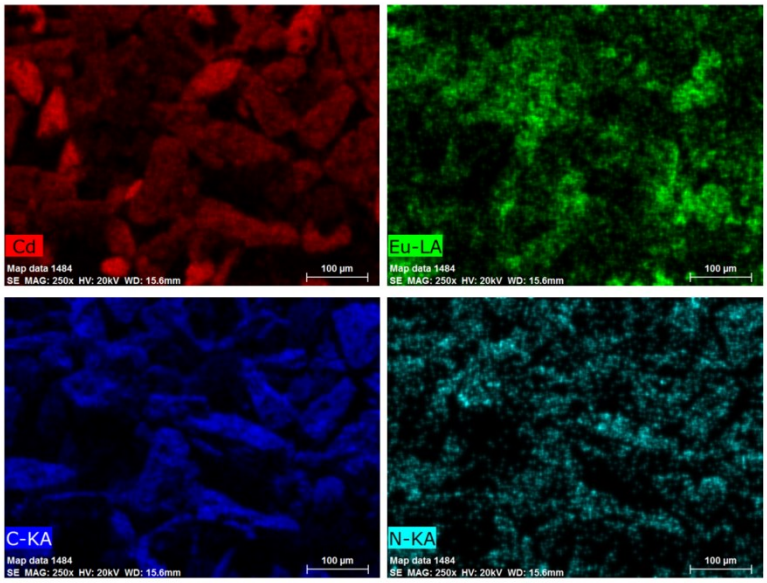

Fig. S13 EDS mapping images of **2A**.

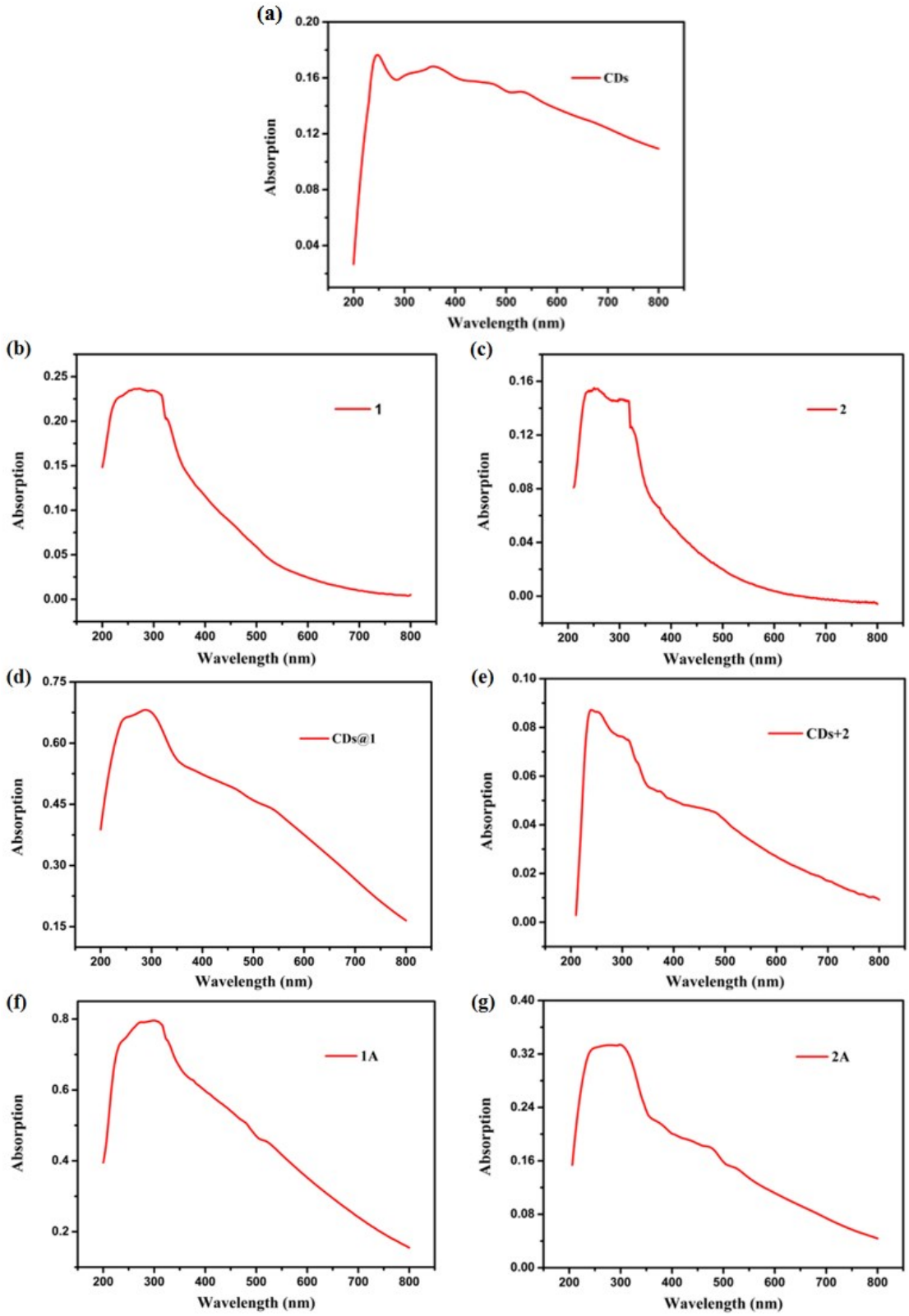

Fig. S14 Solid-state UV-vis absorption spectra of CDs (a), **1** (b), **2** (c), CDs@**1** (d), CDs+**2** (e), **1A** (f) and **2A** (g) at room temperature.

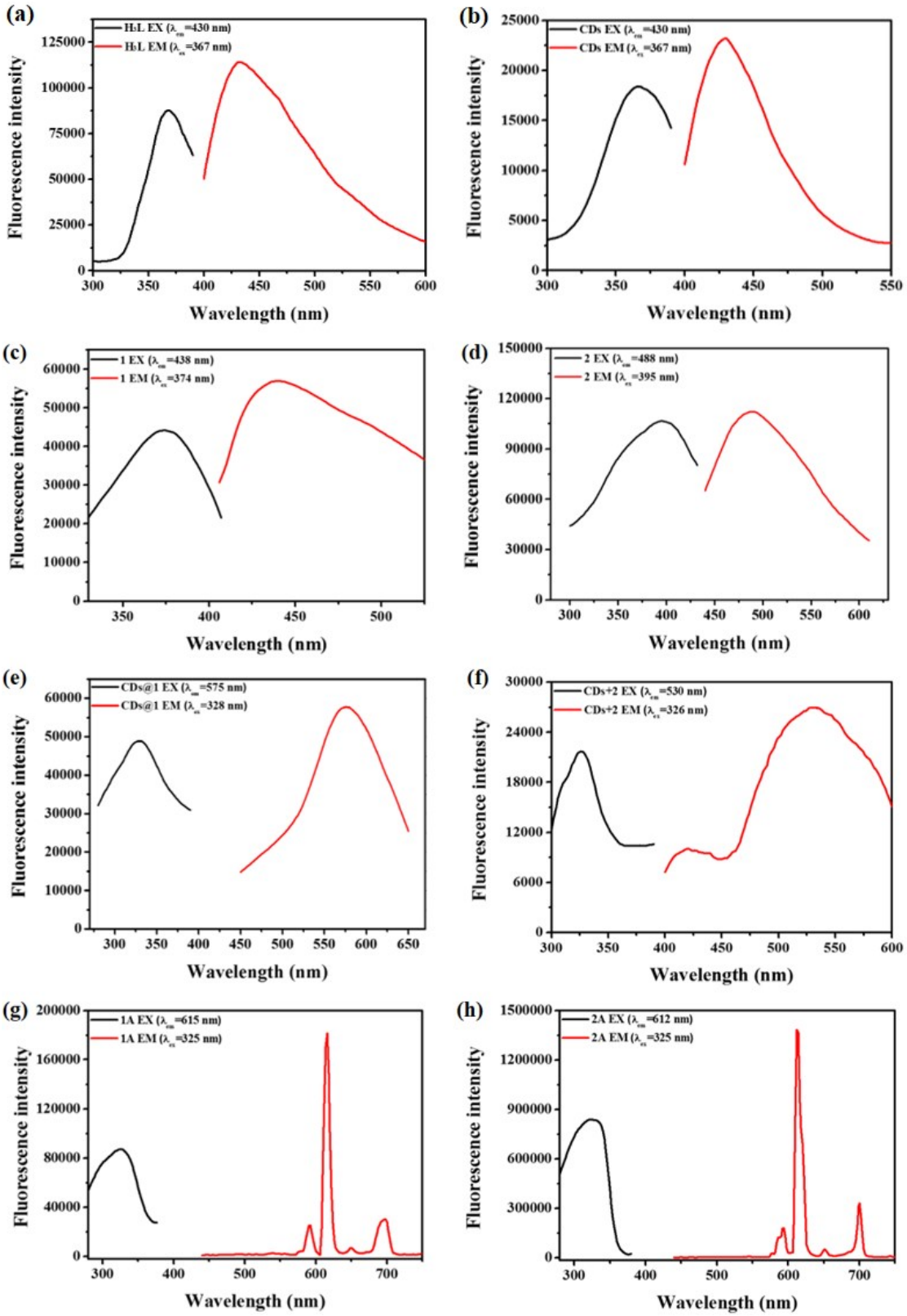

Fig. S15 Solid-state excitation and emission spectra of H_3L (a), CDs (b), **1** (c), **2** (d), CDs@**1** (e), CDs+**2** (f), **1A** (g) and **2A** (h) at room temperature.

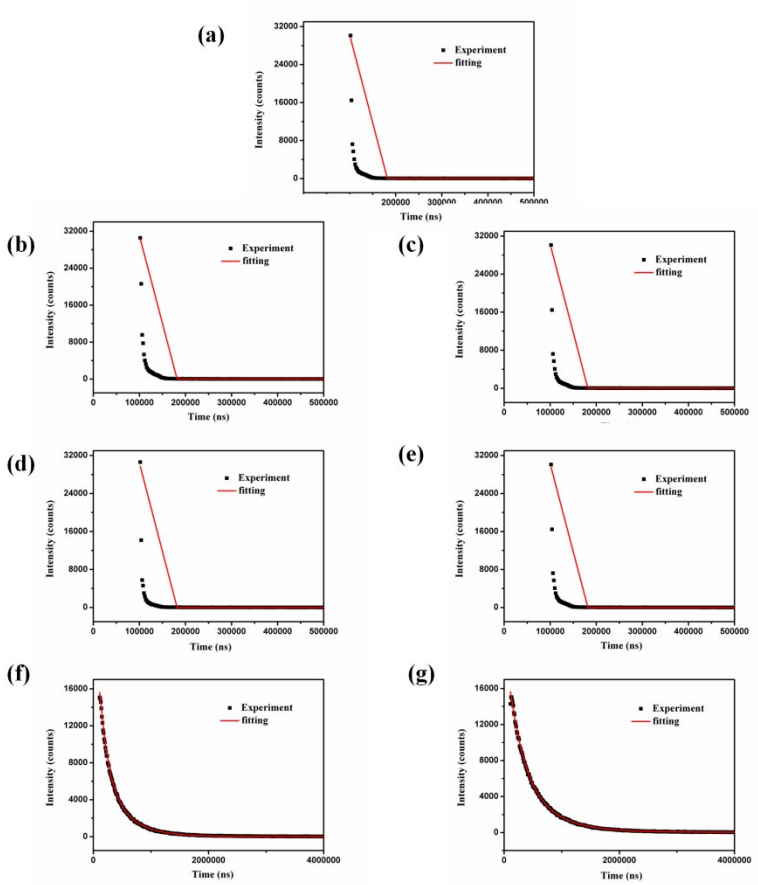

Fig. S16 Fluorescence decay profiles of CDs (a), **1** (b), **2** (c), CDs@**1** (d), CDs+**2** (e), **1A** (f) and **2A** (g) recorded at room temperature.

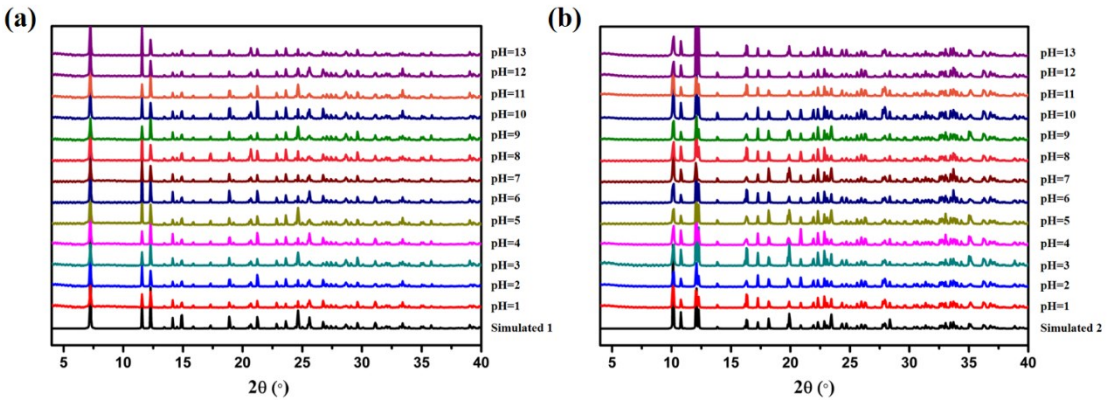

Fig. S17 Powder X-ray diffraction patterns of **1A** and **2A** after the treatment in different pH conditions.

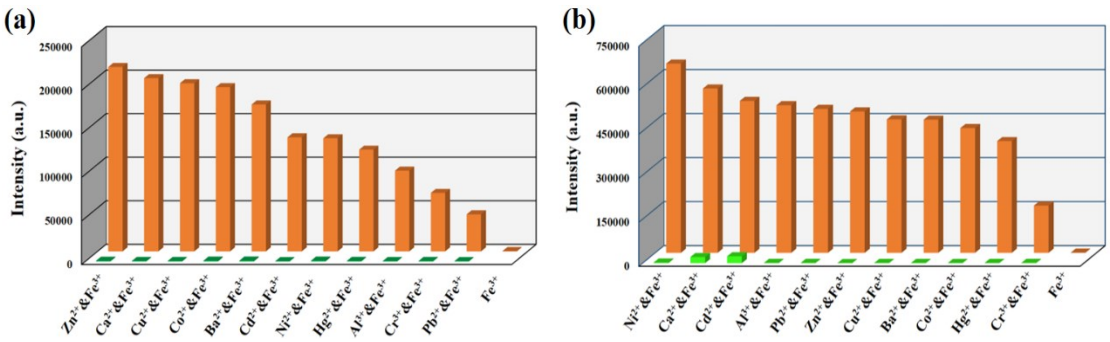

Fig. S18 (a) and (b) The fluorescence intensities of **1A** and **2A** at 612 nm at the addition of various metal ions followed by Fe^{3+} ions. The orange bars represent the intensities in different metal ion aqueous solutions, the green bars represent the intensities in the mixed solutions of Fe^{3+} and other metal ions.

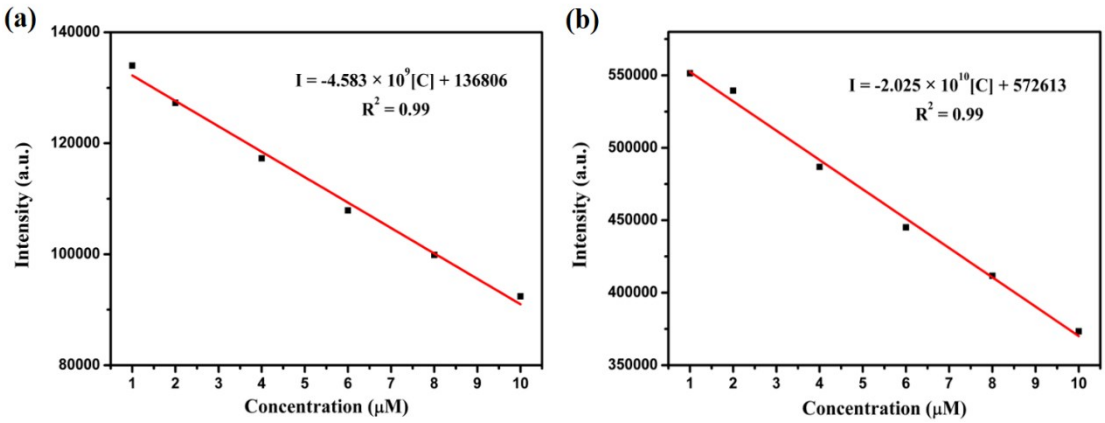

Fig. S19 (a) Relation of fluorescence intensity against Fe^{3+} added into **1A** suspension and their linear fitting curve for the estimation of LOD ($\sigma = 52.42$, $k = 4.583 \times 10^9$ M^{-1}).

Detection Limit = $3\sigma/k$

$= (3 \times 52.42)/4.583 \times 10^9$

$=0.034$ μM

Multiple number of fluorescence spectra (n = 10) were recorded for the blank sample of **1A** suspension. Sample standard deviation σ for the blank probe without the addition of analyte was calculated to be 52.42.

(b) Relation of fluorescence intensity against Fe^{3+} added into **2A** suspension and their linear fitting curve for the estimation of LOD ($\sigma = 65$, $k = 2.025 \times 10^{10}$ M^{-1}).

Detection Limit = $3\sigma/k$

$= (3 \times 65)/2.025 \times 10^{10}$

$= 0.0096$ μM

Multiple number of fluorescence spectra (n = 10) were recorded for the blank sample of **2A** suspension. Sample standard deviation σ for the blank probe without the addition of analyte was calculated to be 65.

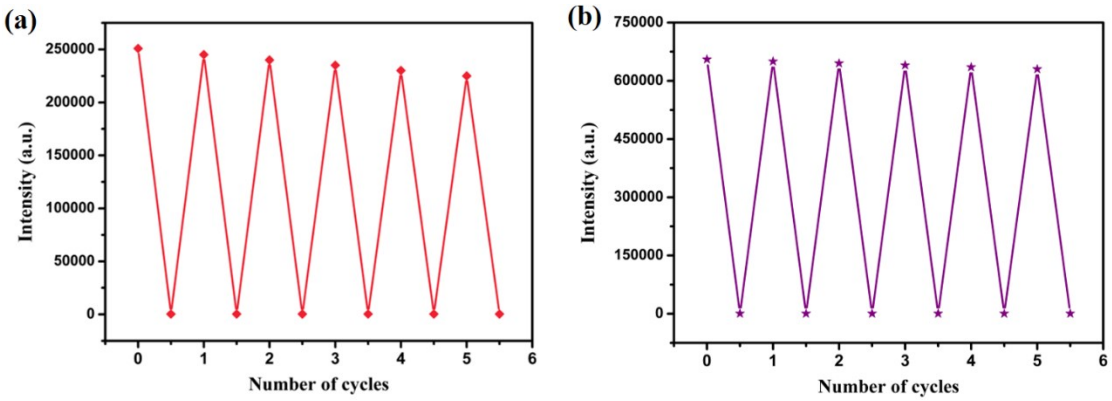

Fig. S20 Cyclic response of **1A** and **2A** for sensing Fe^{3+} (fluorescence intensity at 612 nm.

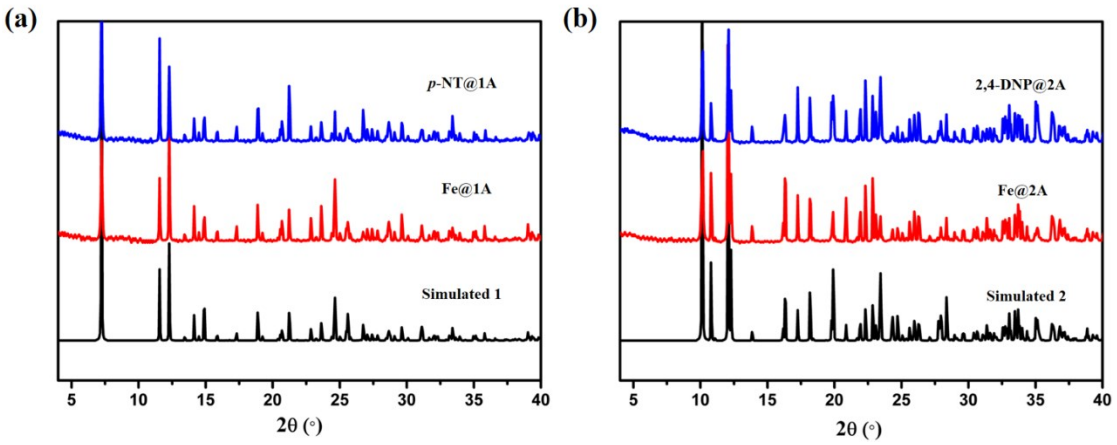

Fig. S21 PXRD patterns of **1A** and **2A** after cyclic sensing Fe^{3+} ions and nitro explosives.

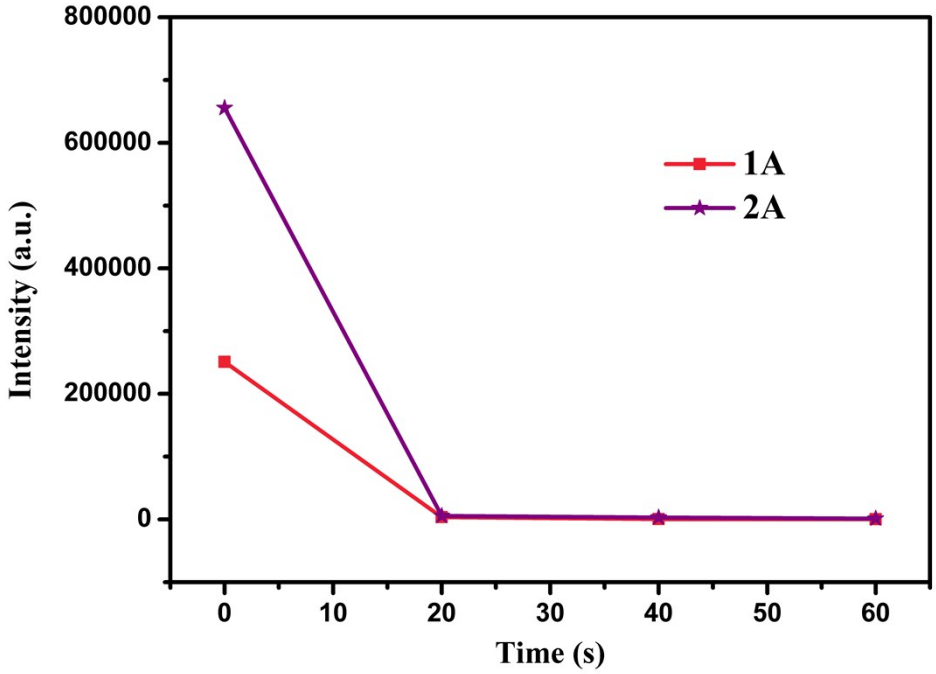

Fig. S22 Variation of fluorescence intensity of **1A** and **2A** with immersion time in analyte solution of Fe^{3+} (1×10^{-2} M^{-1}).

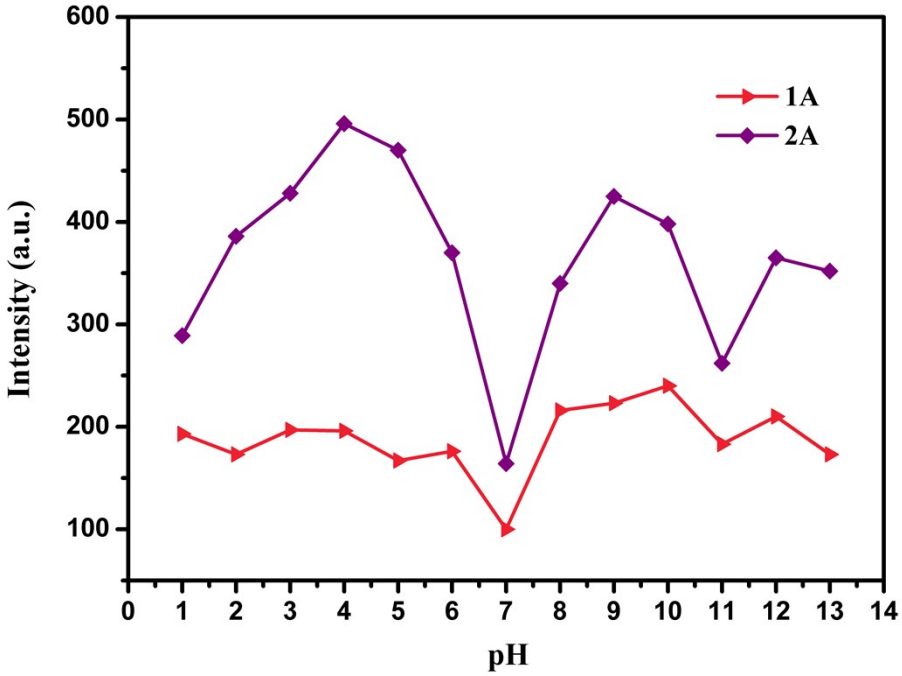

Fig. 23 Effect of pH on the emission intensity of **1A** and **2A** in the presence of Fe^{3+} ions.

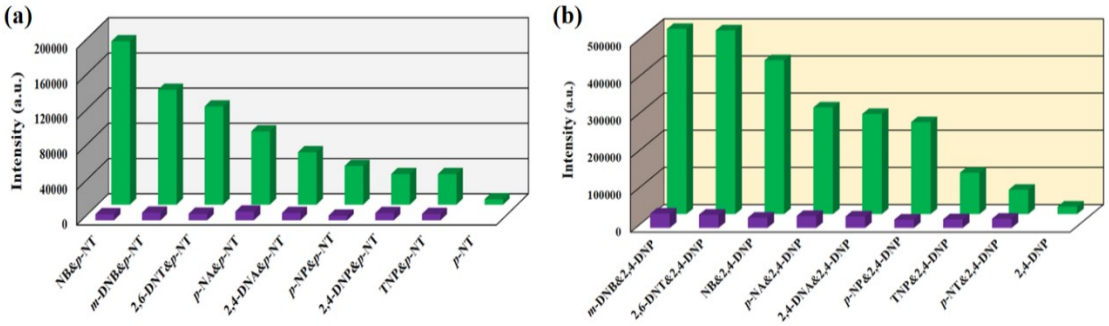

Fig. S24 (a) and (b)The fluorescence intensities of **8A** and **9A** at 612 nm at the addition of various nitro explosives followed by *p*-NT and 2,4-DNP, respectively. The green bars represent the intensities in different nitro explosive aqueous solutions, the purple bars represent the intensities in the mixed solutions of other nitro explosives and *p*-NT and 2,4-DNP, respectively.

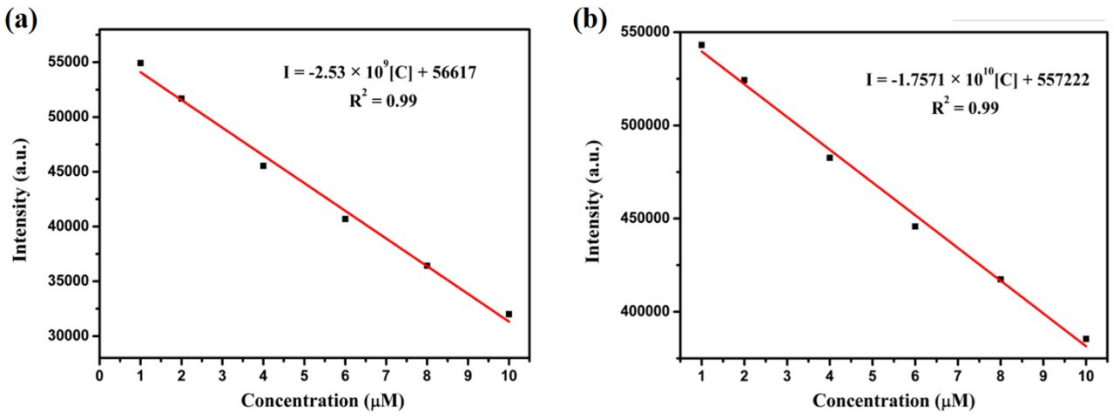

Fig. S25 (a) Relation of fluorescence intensity against *p*-NT added into **8A** suspension and their linear fitting curve for the estimation of LOD ($\sigma = 52.42$, $k = 2.53 \times 10^9$ M^{-1}).

Detection Limit = $3\sigma/k$

$= (3 \times 52.42)/2.53 \times 10^9$

$=0.062$ μM

(b) Relation of fluorescence intensity against 2,4-DNP added into **9A** suspension and their linear fitting curve for the estimation of LOD ($\sigma = 65$, $k = 1.757 \times 10^{10}$ M^{-1}).

Detection Limit = $3\sigma/k$

$= (3 \times 65)/1.757 \times 10^{10}$

$=0.0111$ μM

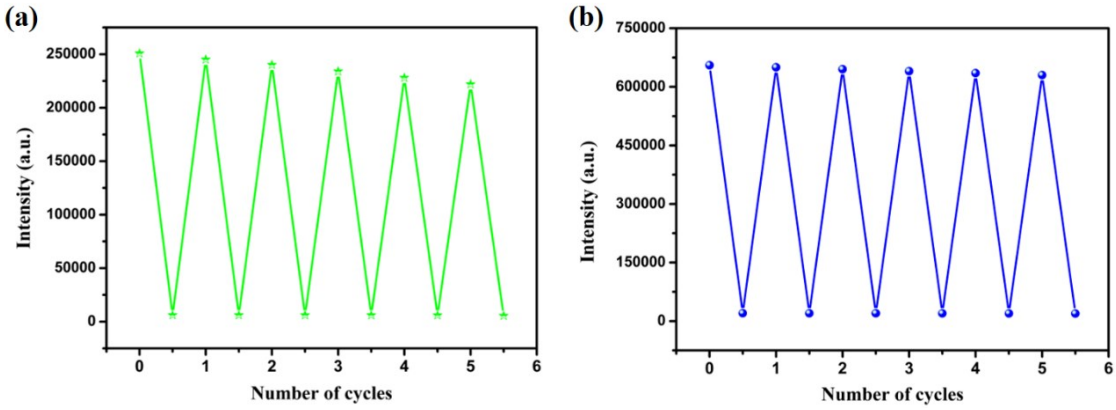

Fig. S26 Cyclic response of **1A** and **2A** for sensing *p*-NT and 2,4-DNP, respectively. (fluorescence intensity at 612 nm).

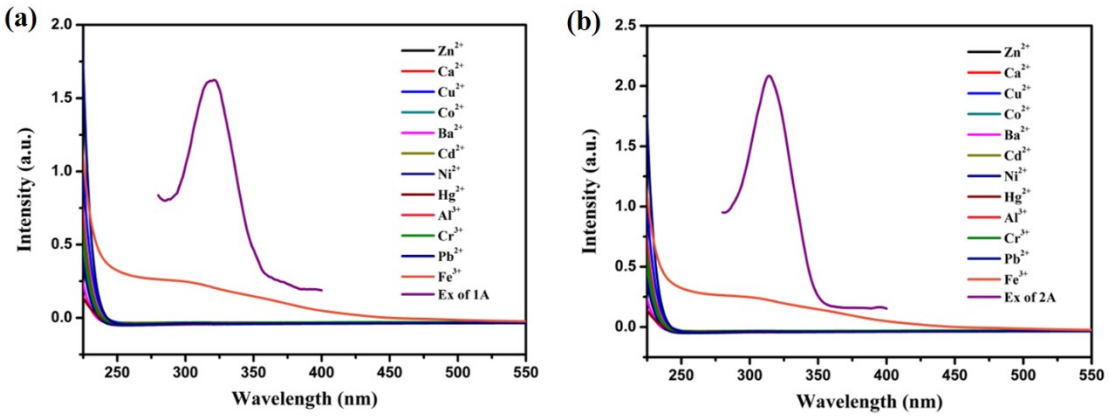

Fig. S27 (a) and (b) The absorption spectra of different cations and the excitation spectrum of **1A** and **2A**.

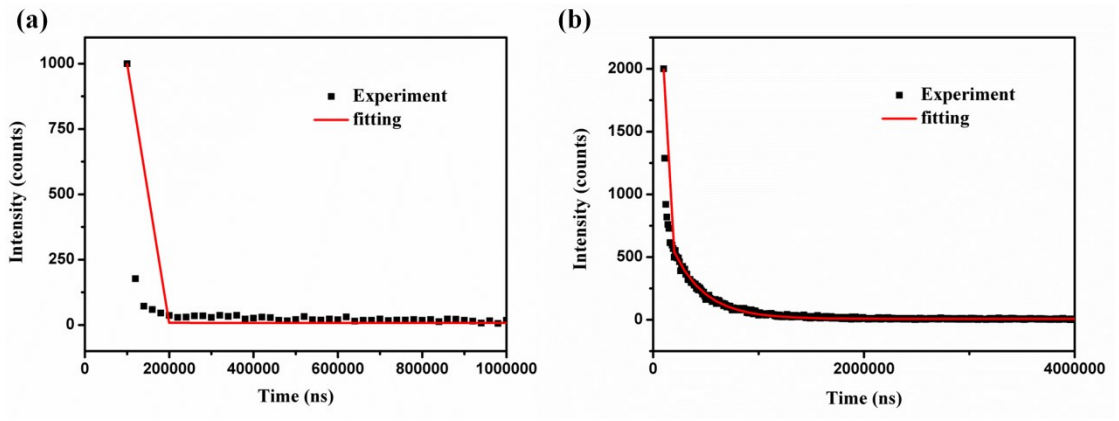

Fig. S28 Fluorescence decay profiles of Fe^{3+}@**1A** (a) and Fe^{3+}@**2A** (b) recorded at room temperature. The $^5D_0$ decay curve of Fe^{3+}@**1A** with emission was monitored at 616 nm (λ_{ex} = 328 nm), τ_1 = 0.012 ms. The $^5D_0$ decay curve of Fe^{3+}@**2A** with emission was monitored at 612 nm (λ_{ex} = 334 nm), τ_1 = 0.013 ms and τ_2 = 0.300 ms.

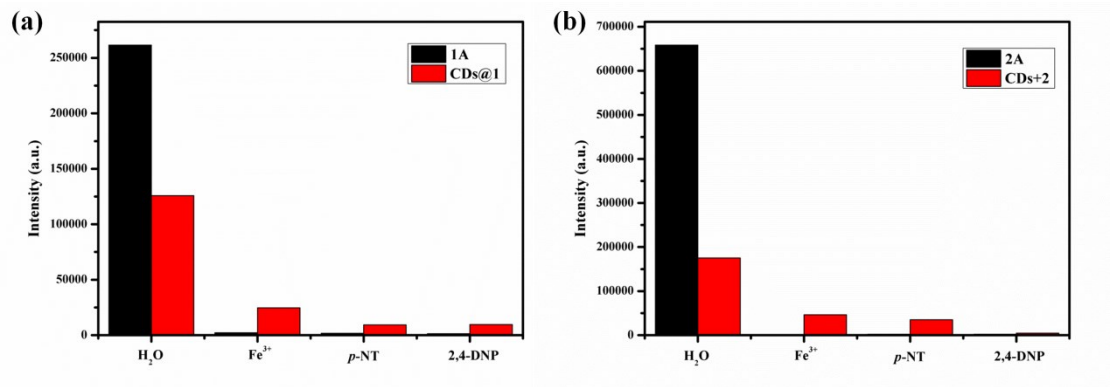

Fig. S29 Sensitivity of (a) **1A** and CDs@**1**, (b) **2A** and CDs+**2**.

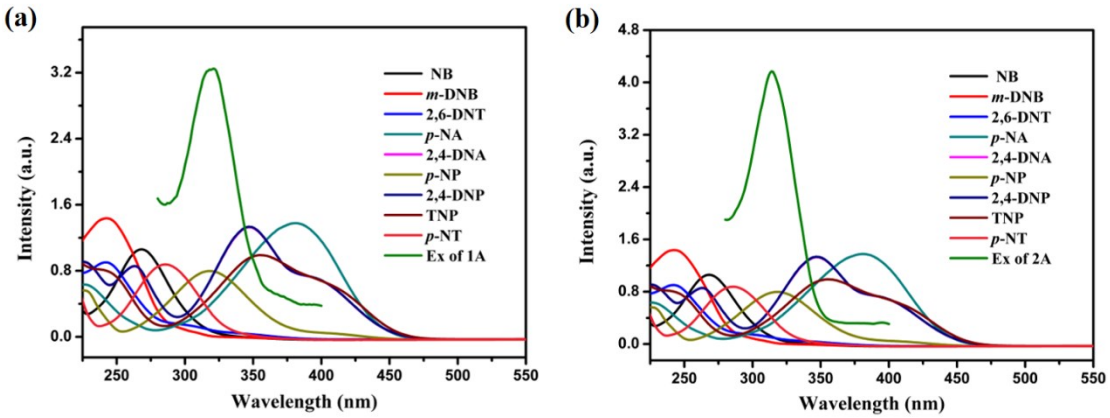

Fig. S30 (a) and (b) The absorption spectra of different nitro explosives and the excitation spectrum of **1A** and **2A**.

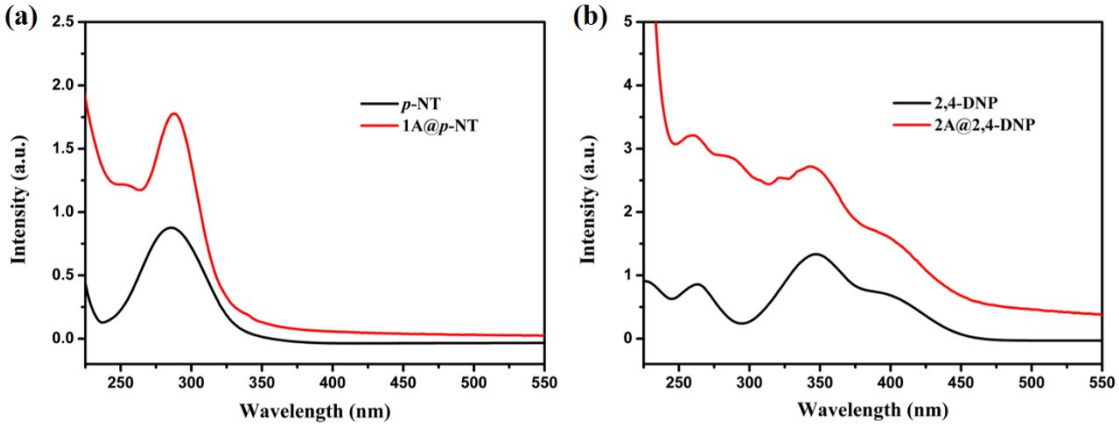

Fig. S31 The UV–vis absorption spectra of **1A** and *p*-NT@**1A** (a), **2A** and 2,4-DNP@**2A** (b).

Table S1. Crystal data and structure refinement for compounds **1**-**2**.

	1	**2**
Formula	$C_{14}H_{8.6}O_{6.8}NCd$	$C_{28}H_{18}O_{15}N_2Cd_3$
Fw (g mol^{-1})	412	959.63
Crystal system	Monoclinic	Monoclinic
Space group	$P2_1/c$	$C2/c$
a (Å)	12.501(3)	15.1651(3)
b (Å)	7.2941(15)	10.8557(2)
c (Å)	15.655(3)	16.4832(3)
V (Å^3)	1395.6(5)	2623.47(9)
Z	4	4
D_{Calc} (mg·cm^{-3})	1.888	2.293
F (000)	772	1736
$\theta range$ (°)	3.09 – 25.00	2.56 –28.31
	-14 ≤ h ≤ 14	-15 ≤ h ≤ 20
Limiting indices	-8 ≤ k ≤ 8	-11 ≤ k ≤ 14
	-18 ≤ l ≤ 18	-21 ≤ l ≤ 21
Refl.Collected / unique	7208/2264	9336/3115
R_{int}	0.0266	0.0161
Data / restraints / parameters	2264/0/199	3115/0/204
GOF	1.160	1.125
R_1 [$I > 2\sigma(I)$]	0.0262	0.0186
wR_2[$I > 2\sigma(I)$]	0.0757	0.0435
R_1 (all data)	0.0292	0.0190
wR_2 (all data)	0.0778	0.0437
Largest diff.peak and hole(e·Å^{-3})	1.020 and -0.477	0.460 and -0.460
CCDC No.	1891845	2073945

Table S2. Selected bond lengths [Å] and angles [°] for compounds **1**-**2**.

1			
O(4)-Cd(1)#1	2.299(3)	O(1)-Cd(1)#3	2.232(3)
O(4)-Cd(1)	2.445(3)	N(1)-Cd(1)#4	2.317(4)
O(2)-Cd(1)#2	2.194(3)	Cd(1)-O(3)	2.354(3)
Cd(1)-O(2)#5	2.194(3)	Cd(1)-O(1)#3	2.232(3)
Cd(1)-O(4)#6	2.299(3)	Cd(1)-N(1)#7	2.317(4)
O(2)#5-Cd(1)-O(1)#3	153.48(14)	O(2)#5-Cd(1)-O(4)#6	83.71(12)
O(1)#3-Cd(1)-O(4)#6	87.80(12)	O(2)#5-Cd(1)-N(1)#7	109.87(13)
O(1)#3-Cd(1)-N(1)#7	93.80(12)	O(4)#6-Cd(1)-N(1)#7	82.60(12)
O(2)#5-Cd(1)-O(3)	89.45(13)	O(1)#3-Cd(1)-O(3)	99.40(13)
O(4)#6-Cd(1)-O(3)	172.76(11)	N(1)#7-Cd(1)-O(3)	97.56(12)
O(2)#5-Cd(1)-O(4)	82.26(12)	O(1)#3-Cd(1)-O(4)	82.94(11)
O(4)#6-Cd(1)-O(4)	126.98(6)	N(1)#7-Cd(1)-O(4)	149.85(12)
O(3)-Cd(1)-O(4)	53.95(10)		

Symmetry transformations used to generate equivalent atoms:

#1 –x, y+1/2, –z+1/2; #2 x, –y+1/2, z–1/2; #3 –x, –y+1, –z; #4 x, y+1, z; #5 x, –y+1/2, z+1/2; #6 –x, y–1/2, –z+1/2; #7 x, y–1, z

2

Cd(1)-O(1)	2.1716(16)	Cd(1)-O(3)#1	2.2627(16)
Cd(1)-O(6)#2	2.2658(16)	Cd(1)-O(5)#3	2.3225(17)
Cd(1)-O(4)#4	2.3260(15)	Cd(1)-O(5)#2	2.545(2)
Cd(2)-O(2)#6	2.2358(16)	Cd(2)-O(2)#6	2.2358(16)
Cd(2)-O(4)#7	2.3329(14)	Cd(2)-O(4)#4	2.3329(14)
Cd(2)-N(1)#7	2.3394(17)	Cd(2)-N(1)#4	2.3394(17)
O(3)-Cd(1)#1	2.2627(16)	O(4)-Cd(1)#8	2.3260(15)
O(4)-Cd(2)#8	2.3329(14)	O(5)-Cd(1)#3	2.3225(17)
O(5)-Cd(1)#9	2.545(2)	O(6)-Cd(1)#9	2.2658(16)
N(1)-Cd(2)#8	2.3394(17)		
O(1)-Cd(1)-O(3)#1	91.18(7)	O(1)-Cd(1)-O(6)#2	120.66(7)
O(3)#1-Cd(1)-O(6)#2	92.87(7)	O(1)-Cd(1)-O(5)#3	92.66(7)
O(3)#1-Cd(1)-O(5)#3	78.24(7)	O(6)#2-Cd(1)-O(5)#3	145.89(7)
O(1)-Cd(1)-O(4)#4	110.63(7)	O(3)#1-Cd(1)-O(4)#4	151.03(5)
O(6)#2-Cd(1)-O(4)#4	92.00(6)	O(5)#3-Cd(1)-O(4)#4	81.80(7)
O(1)-Cd(1)-O(5)#2	171.91(7)	O(3)#1-Cd(1)-O(5)#2	83.36(7)
O(6)#2-Cd(1)-O(5)#2	53.99(6)	O(5)#3-Cd(1)-O(5)#2	92.06(6)
O(4)#4-Cd(1)-O(5)#2	76.57(6)	O(2)-Cd(2)-O(2)#6	107.31(11)
O(2)-Cd(2)-O(4)#7	78.24(7)	O(2)#6-Cd(2)-O(4)#7	85.97(7)
O(2)-Cd(2)-O(4)#4	85.97(7)	O(2)#6-Cd(2)-O(4)#4	78.24(7)
O(4)#7-Cd(2)-O(4)#4	153.26(8)	O(2)-Cd(2)-N(1)#7	152.91(7)
O(2)#6-Cd(2)-N(1)#7	86.11(7)	O(4)#7-Cd(2)-N(1)#7	79.41(6)
O(4)#4-Cd(2)-N(1)#7	120.31(6)	O(2)-Cd(2)-N(1)#4	86.11(7)
O(2)#6-Cd(2)-N(1)#4	152.91(7)	O(4)#7-Cd(2)-N(1)#4	120.31(6)
O(4)#4-Cd(2)-N(1)#4	79.41(6)	N(1)#7-Cd(2)-N(1)#4	92.12(9)

Symmetry transformations used to generate equivalent atoms:

#1 –x+1/2, –y+1/2, –z; #2 x+1, y, z; #3 –x, –y+1, –z; #4 x+1/2, y+1/2, z; #5 –x+1, –y+1, –z; #6 –x+1, y, –z+1/2; #7 –x+1/2, y+1/2, –z+1/2; #8 x–1/2, y–1/2, z; #9 x–1, y, z

Table S3. Fluorescence lifetimes of CDs, **1**, **2**, CDs@**1**, CDs+**2**, **1A**, **2A**, Fe^{3+}@**1A** and Fe^{3+}@**2A**.

Compounds	Fluorescence lifetimes	
CDs	τ_1 = 3.607 μs	τ_2 = 3.270 μs
1	τ_1 = 3.585 μs	τ_2 = 5.022 μs
2	τ_1 = 3.924 μs	τ_2 = 12.283 μs
CDs@**1**	τ_1 = 2.935 μs	-
CDs+**2**	τ_1 = 2.552 μs	-
1A	τ_1 = 0.413 ms	τ_2 = 0.144 ms
2A	τ_1 = 0.584 ms	τ_2 = 0.261 ms
Fe^{3+}@**1A**	τ_1 = 0.012 ms	-
Fe^{3+}@**2A**	τ_1 = 0.013 ms	τ_2 = 0.300 ms

Table S4. The comparison of K_{SV} and detection limit between **1A** and **2A** and other reported fluorescent chemosensors for detecting of Fe^{3+} ions.

MOFs	K_{SV} (M^{-1})	Detection limits (μM)	Reference
1A	9.269×10^4	0.034	This work
2A	6.329×10^4	0.0096	This work
$[Zn_3(L_1)_2(bipy)(\mu_3\text{-}OH)_2]\cdot 3H_2O$	2.3×10^4	-	[1]
$[Zr_6O_4(OH)_8(H_2O)_4(L_2)_2]$	1.66×10^4	0.0396	[2]
$[Zn_2(bptc)(H_2O)]\cdot(4,4'\text{-}bipy)_{0.5}$	2.826×10^4	8.5	[3]
$[Cd(L_3)\text{-}(BPDC)]\cdot 2H_2O$	3.64×10^4	2.21	[4]
$[Cd(L_3)(SDBA)(H_2O)]\cdot 0.5H_2O$	3.59×10^4	7.14	[4]
[Cd(5-asba)(bimb)]	1.78×10^4	-	[5]

H_2L_1 = 9H-carbazolyl-3,6-dicarboxylic acid;

H_2L_2 = 4,4′,4″,4‴-(4,4′-(1,4-phenylene)bis(pyridine-6,4,2-triyl))-tetrabenzoate;

H_4bptc = 2,4,4′,6-biphenyl tetracarboxylic acid;

L_3 = 4,4′-(2,5-bis(methylthio)-1,4-phenylene)dipyridine;

H_2BPDC = 4,4′-biphenyldicarboxylic acid;

H_2SDBA = 4,4′-sulfonyldibenzoic acid;

$H_2$5-asba = 2-amino-5-sulfobenzoic acid;

bimb = 1,4-bis(1H-imidazol-1-yl)butane.

Table S5. The comparison of K_{SV} and detection limit between **1A** and other reported fluorescent chemosensors for detecting of *p*-NT.

MOFs	K_{SV} (M^{-1})	Detection limits (μM)	Reference
1A	3.57×10^5	0.062	This work
$[Cd(DBCD)(1,3\text{-bib})]\cdot(H_2O)_2$	6.8×10^4	-	[6]
$[Zn(DBCD)(1,4\text{-bib})]\cdot(H_2O)_2$	1.5×10^5	-	[6]
$[Cd_{1/2}(L_4)_{1/3}(bib)_{1/2}(H_2O)]$	1.7×10^5	-	[7]
$[Cd_2(HL_4)_2(bibp)_2]\cdot 3H_2O$	1.0×10^5	-	[7]
534-MOF-Tb	7.90×10^4	320	[8]
$[Zn(tta)_{0.5}(m\text{-bimb})]\cdot H_2O$	1.78×10^4	-	[9]

H_2DBCD = N,N'-dioxide 3,3'-benzo(c)cinnoline dicarboxylic acid;

H_3L_4 = trisIJp-carboxyphenyl)phosphane oxide;

bib = 1,4-bisIJimidazol-1-yl)benzene;

bibp = 4,4′-bisIJimidazol-1-yl)biphenyl;

H_4tta = terphenyl-4,2″,5″,4′-tetracarboxylic acid;

m-bimb = 1,3-bis(imidazol-1-ylmethyl)benzene.

Table S6. The comparison of K_{SV} and detection limit between **2A** and other reported fluorescent chemosensors for the detecting of 2,4-DNP.

MOFs	K_{SV} (M^{-1})	Detection limits (μM)	Reference
2A	5.456×10^4	0.0111	This work
$(CH_3)_2NH_2)_6[Cd_5(L_5)_4]\cdot H_2O\cdot 3DMF$	2.37×10^4	4.56	[10]
$(NH_2(CH_3)_2)[Zn_4(ddn)_2(COO)(H_2O)_4]$ ·solvent	8.93×10^3	6.08	[11]
$[Nd(L^1)(NO_3)_3]\cdot 2DMF$	7.00×10^3	0.72	[12]
$[Sm(L^1)(NO_3)_3]\cdot 2DMF$	5.90×10^3	0.70	[12]
$(PFBHC)_2Ir(acac)$	1.58×10^3	89	[13]

H_4L_5 = terphenyl-3,3″,5,5″-tetracarboxylic acid;

H_4ddn = 3,5-di(3,5-dicarboxylphenyl)nitrobenzene;

PFBHC = 9,90-((2-(pyridin-2-yl)-9H-fluorene-9,9-diyl)bis(hexane-6,1-diyl))bis(9H-carbazole).

References

[1] J.-L. Du, X.-Y. Zhang, C.-P. Li, J.-P. Gao, J.-X. Hou, X. Jing, Y.-J. Mu and L.-J. Li, *Sens. Actuators*, *B*, 2018, **257**, 207-213.

[2] B. Wang, Q. Yang, C. Guo, Y. X. Sun, L.-H. Xie and J.-R. Li, *ACS Appl. Mater. Interfaces*, 2017, **9**, 10286-10295.

[3] J. Sun, P. Zhang, H. Qi, J. Jia, X. D. Chen, S. B. Jing, L. Wang and Y. Fan, *Inorg. Chimica Acta*, 2018, **469**, 298-305.

[4] S. G. Chen, Z. Z. Shi, L. Qin, H. L. Jia and H. G. Zheng, *Cryst. Growth Des.*, 2017, **17**, 67-72.

[5] Y.-J. Yang, M.-J. Wang and K.-L. Zhang, *J. Mater. Chem. C,* 2016, **4**, 11404-11418.

[6] X.-T. Zhang, H.-T. Chen, B. Li, G.-Z. Liu and X.-Z. Liu, *J. Solid State Chem.*, 2018, **267**, 28-34.

[7] L. Q. Huo, J. Zhang, L. L. Gao, X. Q. Wang, L. M. Fan, K. G. Fang and T. P. Hu, *CrystEngComm*, 2017, **19**, 5285-5292.

[8] M. Chen, W.-M. Xu, J.-Y. Tian, H. Cui, J.-X. Zhang, C.-S. Liu and M. Du, *J. Mater. Chem. C*, 2017, **5**, 2015-2021.

[9] X.-T. Zhang, H.-T. Chen, B. Li, G.-Z. Liu and X.-Z. Liu, *Dalton Trans.*, 2018, **47**, 1202-1213.

[10] L. Lu, J. Wu, J. Wang, J.-Q. Liu, B.-H. Li, A. Singh, A. Kumar and S. R. Batten, *CrystEngComm*, 2017, **19**, 7057-7067.

[11] A. Q. Ma, J. Wu, Y. T. Han, F. M. Chen, B. H. Li, S. G. Cai, H. Huang, A. Singh, A. Kumar and J. Q. Liu, *Dalton Trans.*, 2018, **47**, 9627-9633.

[12] M. Kose1, H. Kırpık1, A. Kose and M. Karabork, *Appl. Organometal Chem.*, 2019, **33**, 1-9.

[13] Q. H. Ma, W. Y. Dong, Z. H. Ma, X. L. Lv, Y. W. Li and Q. Duan, *Mater. Letters*, 2019, **249**, 120-123.